*Biological Journal of the Linnean Society*, 2020, **130**, 756–770. With 5 figures.

# Hitchhiking consequences for genetic and morphological patterns: the influence of kelp-rafting on a brooding chiton

P. M. SALLOUM[1,*], P. DE VILLEMEREUIL[2], A. W. SANTURE[1], J. M. WATERS[3] and S. D. LAVERY[1,4]

[1]*School of Biological Sciences, University of Auckland, Auckland, New Zealand*
[2]*EPHE PSL University, Institut de Systématique, Evolution et Biodiversité, UMR 7205, CNRS, MNHN, Sorbonne Université, Paris, France*
[3]*Department of Zoology, University of Otago, Dunedin, New Zealand*
[4]*Institute of Marine Science, Leigh Marine Laboratory, University of Auckland, Warkworth, New Zealand*

*Received 23 December 2019; revised 1 May 2020; accepted for publication 5 May 2020*

*Onithochiton neglectus* is a morphologically variable, brooding chiton inhabiting coastal reefs throughout New Zealand and its Sub-Antarctic Islands. Southern *O. neglectus* populations are typically associated with buoyant kelp (*Durvillaea* spp.) and are potentially connected via kelp-rafting. Northern *O. neglectus* populations are less likely to raft, due to lower numbers of *Durvillaea* in northern New Zealand. To test for the impact of kelp-rafting on the spatial distribution of variation in *O. neglectus*, we undertook a combined analysis of morphological and genetic variation across the range of the species. Geometric morphometrics were used to assess shell shape. We detected a northern vs. southern split in shell shape, corresponding to the frequency of the *O. neglectus*/*Durvillaea* spp. association. To assess *O. neglectus* genetic patterns across New Zealand, we estimated phylogenetic trees with nuclear (ITS) and mitochondrial (*COI* and 16S) markers, which revealed distinct northern and southern lineages, and an additional lineage in central New Zealand. Neither the morphological nor genetic groups match existing *O. neglectus* subspecies, but are concordant with the patterns of association of *O. neglectus* with *Durvillaea*. We suggest that shell shape may be linked to *O. neglectus*' regionally variable ecological association with kelp holdfasts.

ADDITIONAL KEYWORDS: *Durvillaea antarctica* – elliptic Fourier analysis – geometric morphometrics – molecular divergence – morphology – mtDNA – New Zealand – *Onithochiton* – phylogeography – shape-analysis – shell shape.

## INTRODUCTION

Understanding the processes that determine the spatial distribution of biological variation can help to predict responses to environmental change. Such understanding is particularly important in the face of global change. In the marine environment in particular, ocean warming is driving profound changes in ecosystems by affecting habitat-forming species such as kelp, leading to a shift in the spatial distribution not only of those species, but of numerous life forms associated with these keystone taxa (Christie *et al.*, 2019; Smale *et al.*, 2019). In New Zealand, the bull kelp *Durvillaea antarctica* (Chamisso) Hariot, 1892, has been shown to be an important driver of connectivity among populations of different marine species inhabiting the Sub-Antarctic Islands and New Zealand's South Island, as these species may hitchhike on the holdfasts of *D. antarctica* cast adrift in the sea (Fraser *et al.*, 2011; Cumming *et al.*, 2014; González-Wevar *et al.*, 2018; Waters *et al.*, 2018a). Dispersal promoted by rafting on *D. antarctica* is expected to increase connectivity among the affected populations compared to populations lacking kelp-rafting (Nikula *et al.*, 2011). As a result of differential connectivity and selection pressures experienced by coastal benthic populations, divergent adaptations can emerge in populations with and without the influence of kelp

*Corresponding author. E-mail: psal591@aucklanduni.ac.nz

rafting. Assessing such connectivity patterns helps to understand the spatial distribution of variation and the responses of individuals to their environment.

The New Zealand chiton *Onithochiton neglectus* Rochebrune, 1881, is a low intertidal species that often inhabits the holdfasts of benthic *Durvillaea* kelp (both *D. antarctica* and the closely related *D. poha*). *Onithochiton neglectus* has frequently been observed rafting on detached individuals of these kelp species, being transported for long distances among New Zealand's Sub-Antarctic Islands and the South Island (Creese, 1986; Thiel & Haye, 2006; Nikula *et al.*, 2012; López *et al.*, 2017, 2018; Waters *et al.*, 2018a). Previous studies have identified shared mitochondrial haplotypes between *O. neglectus* in the South Island and the Sub-Antarctic Islands, providing evidence that connectivity among *O. neglectus* populations is promoted by rafting on *Durvillaea* in the southern region (Nikula *et al.*, 2012; Waters *et al.*, 2018a), but populations north of Dunedin (45.88°S, 170.50°E) remain to be assessed. Due to *O. neglectus*' brooding behaviour and release of short-lived larvae with limited mobility (Creese, 1986), little connectivity is expected where kelp-rafting is infrequent (Thiel & Haye, 2006; Lopez *et al.*, 2017, 2018).

*Onithochiton neglectus* is endemic to New Zealand, and has a wide latitudinal range extending from the subtropical waters of the northern North Island to the cold waters surrounding the Sub-Antarctic Islands (Powell, 1979; O'Neill, 1985; Creese, 1986). Ecological associations between *O. neglectus* and *Durvillaea* kelps occur predominantly at the southern end of the *O. neglectus* distribution (New Zealand's South Island and Sub-Antarctic Islands), contrasting with the northern portion of the distribution, where *D. poha* does not occur, *D. antarctica* is relatively rare and *O. neglectus* is predominantly found independently under rocks. Because of its broad distribution, differential association with kelp and brooding behaviour, *O. neglectus* is an ideal system for a comparative study considering the extent to which kelp-rafting can homogenize genetic and morphological variation.

Morphologically, *O. neglectus* is highly variable throughout its distribution, with a diversity of colours and shell sculptures (O'Neill, 1985). Such variability may have been responsible for the great confusion in past classifications of this species, resulting in 18 synonyms (O'Neill, 1984, 1985). Currently, *O. neglectus* is considered to comprise two subspecies, *Onithochiton neglectus neglectus* Rochebrune, 1881 and *Onithochiton neglectus subantarcticus* Suter, 1906. The former is found in the North, South and Stewart Islands. In contrast, *O. neglectus subantarcticus* has a distribution restricted to the Sub-Antarctic Antipodes Islands, Auckland Islands, Campbell Islands and possibly Bounty Islands, and is characterized by minor, but stable, geographical differences in morphology, including smooth, dark shells (O'Neill, 1984, 1985). However, the discovery of shared mitochondrial haplotypes throughout the southern region challenges the existence of an *O. neglectus* subspecies restricted to some of the Sub-Antarctic Islands (O'Neill, 1985; Nikula *et al.*, 2012).

To assess the impact of kelp association on the current spatial distribution of variation in this species, we examined both genetic and shell shape variation in *O. neglectus* populations throughout its distribution. In particular, shell shape differences could also be related to the level of wave exposure experienced by animals, as a kelp holdfast is more sheltered than the under-boulder reef environment. We hypothesize that ecological constraints of kelp association, and enhanced genetic exchange mediated by rafting, may influence the morphological differentiation of southern (epifaunal) populations, when compared to the northern populations. Furthermore, we hypothesize that northern populations are more genetically structured than southern populations, due to the reduced occurrence of kelp-rafting and hence probably lower connectivity between populations.

For measuring shape variation across populations, geometric morphometrics methods are particularly useful (Adams *et al.*, 2004; Cadrin, 2010; Cooke & Terhune, 2015; Mooney & Kingsford, 2016). A large number of studies have utilized landmark-based approaches, in which corresponding structural points among specimens are chosen to be landmarks, and changes in the relative coordinates of these points show shape changes in the structure among those specimens (Cooke & Terhune, 2015). However, in study systems such as *O. neglectus*, the whole outline of a structure may contain the targeted shape information, and in such cases, elliptic Fourier analysis is an effective alternative, as it extracts shape information from closed contours (Kuhl & Giardina, 1982; Iwata & Ukai, 2002; Sheets *et al.*, 2006). As the chiton shell valves vary in overall shape, and have few hard landmarks on the exterior face, we used elliptic Fourier analysis to assess shell shape variation across *O. neglectus* populations.

In conjunction with the morphometric analyses, we generated phylogenetic trees using two mitochondrial DNA markers (*COI* and 16S rRNA) and one nuclear marker (ITS-1) for the same individuals from which the shell shape data were collected, in order to describe the broad phylogeographical structure within the species. Finally, we considered both shell shape and molecular data in combination, aiming to test for concordance among morphology, genetics, taxonomy and association with kelp, in order to better understand the distribution of variation within *O. neglectus*.

## MATERIAL AND METHODS

### SAMPLING DESIGN

Sixteen populations of *O. neglectus* distributed across New Zealand and its Sub-Antarctic Islands were included in this study (Figure 1; Table 1). Ten southern populations were sampled in 2009 for a previous study (Nikula *et al.*, 2012), and individuals from these samples were kindly made available by the authors. These locations were Christchurch, Dunedin, Akatore, Curio Bay, Stewart Island, Auckland Islands, Campbell Islands, Antipodes Islands, Bounty Islands and Chatham Islands. The other populations were sampled in 2017 and 2018, comprising six populations from the North Island (Russell, Auckland, Coromandel, East Cape, Wellington and Cape Palliser) and two re-sampled populations from the South Island (Christchurch and Dunedin). On the North Island, single individuals were manually collected from the underside of boulders at least 3 m apart, across the extension of the shore, in the shallow intertidal to upper subtidal zone during spring low tides. Neither *D. antarctica* nor *D. poha* occur at these locations. On the South Island and the Sub-Antarctic Islands, individuals were collected from the holdfasts of *Durvillaea* specimens that were either beach cast or prised off rock at low tide (Supporting Information, Table S1). To ensure that beach-cast chiton samples were of local origin, kelp was checked for the presence of goose-barnacles, whose size indicates rafting time in the ocean, and only samples that were afloat for short periods of time were included (Fraser *et al.*, 2011). Samples were preserved in 70–95% ethanol after collection.

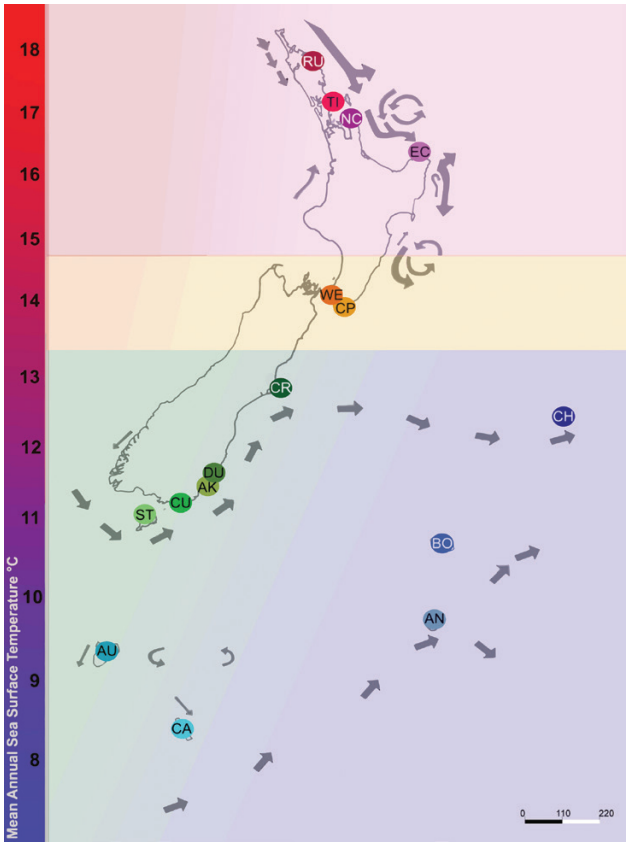


**Figure 1.** Sampled *Onithochiton neglectus* populations shown with a schematic representation of New Zealand marine circulation (indicated by arrows) and approximate mean annual sea surface temperature gradient (indicated by the gradient bar on the left). Sample codes are given in Table 1. The three large horizontal bands identify three distinct genetic clades identified in this study. The Chatham Islands were included in the Sub-Antarctic Islands region in this study.

### QUANTIFYING SHELL SHAPE VARIATION WITH GEOMETRIC MORPHOMETRICS

Shell shape analysis was undertaken on the exterior face of three valves from each individual, photographed separately and analysed individually: the head (valve i), the fourth (valve iv) and the tail (valve viii) (Supporting Information, Figure S1). The head and the tail valves have a unique shape, and are commonly used in chiton taxonomic classifications (Baxter & Jones, 1981; O'Neill, 1984, 1985). All the other valves may vary in size, but have a similar shape, so only the fourth valve was used as representative. Broken valves were excluded from the analysis.

After photographing the valves, Adobe Photoshop CC 2015 was used to measure the valve area. Quantification of shell shape via elliptic Fourier analysis was performed with SHAPE v.1.3 (Iwata & Ukai, 2002). The resulting coefficients were analysed with a principal component analysis (PCA) using the SHAPE v.1.3 package PrinComp, which outputs principal component scores that can be used as quantitative observations of shape (Iwata & Ukai, 2002). The principal component scores were plotted in R Studio v.1.1.453, with the package ggplot2 (Wickham, 2016). Subsequently, the package vegan v.2.5-4 (Oksanen *et al.*, 2019) was used to compute Euclidean distances between points in the PCA space, using the first principal component score of each valve. These 'shape' Euclidean distances were then used to compute and plot shape centroids for each population, also using vegan.

To check if differences in shape were attributable to allometry (Outomuro & Johansson, 2017), Spearman tests of correlation among valve area (representing size) and principal component scores (representing shape) were undertaken using the R package ggpubr v.0.2 (Kassambara, 2018). In addition, a subset of the

**Table 1.** Sampled populations and sample sizes

| Regional group | Population (code) | *COI* sample size | Shape sample size (fourth/head/tail) | Shell pattern | Previous subspecies designation |
|---|---|---|---|---|---|
| Northern North Island | Russell (RU) | 10 | 5/13/13 | Ringed | *O. neglectus neglectus* |
| Northern North Island | Auckland (TI) | 9 | 7/14/14 | Ringed | *O. neglectus neglectus* |
| Northern North Island | Coromandel (NC) | 10 | 6/10/11 | Ringed | *O. neglectus neglectus* |
| Northern North Island | East Cape (EC) | 9 | 8/9/8 | Ringed | *O. neglectus neglectus* |
| Central New Zealand | Wellington (WE) | 13 | 12/16/16 | Ringed | *O. neglectus neglectus* |
| Central New Zealand | Cape Palliser (CP) | 9 | 5/9/8 | Ringed | *O. neglectus neglectus* |
| South Island | Christchurch (CR) | 6 | 8/8/9 | Ringed/smooth | *O. neglectus neglectus* |
| South Island | Dunedin (DU) | 16 | 17/21/17 | Ringed/smooth | *O. neglectus neglectus* |
| South Island | Akatore (AK) | 7 | 7/10/8 | Ringed | *O. neglectus neglectus* |
| South Island | Curio Bay (CU) | 4 | 5/6/6 | Ringed | *O. neglectus neglectus* |
| South Island | Stewart Island (ST) | 7 | 9/10/10 | Ringed | *O. neglectus neglectus* |
| Sub-Antarctic Islands | Auckland Islands (AU) | 10 | 10/11/10 | Smooth | *O. neglectus subantarcticus* |
| Sub-Antarctic Islands | Campbell Islands (CA) | 7 | 7/8/9 | Smooth | *O. neglectus subantarcticus* |
| Sub-Antarctic Islands | Antipodes Islands (AN) | 7 | 5/7/7 | Smooth | *O. neglectus subantarcticus* |
| Sub-Antarctic Islands | Bounty Islands (BO) | 8 | 6/11/9 | Smooth | *O. neglectus subantarcticus* |
| Sub-Antarctic Islands* | Chatham Islands (CH)* | 7 | 8/8/6 | Ringed/smooth | *O. neglectus neglectus* |

Population codes are the same as in Figure 1. COI sample size corresponds to the number of individuals from each population included in the genetic analyses for the cytochrome oxidase I marker. Shape sample size corresponds to the number of individuals included in the shell shape analysis for each of the valves (fourth, head and tail). The "Ringed" shell pattern corresponds to the presence of colours and rings in the valves, as opposed to the "smooth" and dark pattern without visible rings. The previous subspecies classification is based on O'Neill (1985).

*The Chatham Islands were included in the Sub-Antarctic Islands region for the purposes of this study.

fourth valve including only similar-sized individuals was used in a PCA. This enabled us to check if the shape patterns displayed in the dataset with similar-sized individuals are the same as those displayed in the complete dataset. If the patterns remain similar, shape changes are likely to be due to the existence of different morphogroups, and not completely attributable to allometry. Further details of the valve photography and shell shape analyses are available in the Supporting Information.

### Analyses of current and historical genetic patterns

For the genetic analyses, the mitochondrial gene cytochrome oxidase subunit I (*COI*) was used as the principal molecular marker. We attempted to perform the shell shape and the genetic analyses on the same individuals. However, some samples had broken valves or had unsuccessful DNA amplifications. For analyses of the fourth valve, 125 samples were included (90 of which also have *COI* data); for the head valve, 170 samples were included (122 of which have *COI* data); and for the tail valve, 161 samples were included (116 of which have *COI* data). Of all individuals included in the shell shape analyses, 107 have data for all three valves (77 of which have *COI* data).

DNA was extracted from a small piece of the muscular foot (around 2 $mm^3$) using the Gentra Puregene Kit (Qiagen), following the manufacturer's recommendations, except that the cell lysis step was performed at 60 °C for 4 h, and an additional 70% ethanol wash step was undertaken. DNA concentration and purity were checked with a NanoPhotometer N60 (Implen) and visually inspected by electrophoresis (0.8% agarose in 0.5× TBE buffer).

A fragment of the mitochondrial *COI* region was amplified by polymerase chain reaction (PCR) using the primers HCO and LCO (Folmer *et al.*, 1994) and then sequenced (see Supporting Information for details). *COI* sequences were aligned in Geneious v.10.2.3 using the Geneious alignment option. Sequences were automatically trimmed with an error probability limit of 0.5 and maximum length of 615 bp after trim, and manually annotated. An *Onithochiton hirasei* Pilsbry, 1901, *COI* sequence (AB714507) from GenBank was added to the alignment, where it was trimmed to the same length as *O. neglectus* sequences, and used as the outgroup in the phylogenetic analysis.

To assess genetic differentiation among populations, $\Phi_{ST}$ output from analyses of molecular variance (AMOVAs), as well as population pairwise $\Phi_{ST}$, were estimated in Arlequin 3.5.2.2 (Excoffier & Lischer, 2010). A Bonferroni sequential correction for multiple tests was applied on the pairwise $\Phi_{ST}$. PopART was used to build a neighbour joining haplotype network (Leigh & Bryant, 2015). Beast 2 (Bouckaert *et al.*, 2014) was used to estimate divergence times on a *COI*

phylogenetic tree, and to estimate past demographic events with an extended Bayesian skyline plot (EBSP) (Bouckaert *et al.*, 2014). A Beast Model Test (Bouckaert & Drummond, 2017) was used to estimate the site model on all runs. Divergence dating runs were done with a Yule Model prior, and EBSP runs with a coalescent extended Bayesian skyline model. All other priors were left at the default settings. Clock rates were set according to the best available estimates of closely related chiton mutation rates, which include upper and lower bounds in rates of nucleotide divergence for the *COI* gene using several suborder Chitonina sister species (in the same suborder as *O. neglectus*) separated by the Panama Isthmus emergence as a calibration point (García-Ríos *et al.*, 2014). The upper bound divergence rate is 3.7%/Myr (clock rate set to 0.0185) and the lower bound divergence rate is 1.1%/Myr (clock rate set to 0.0055). All runs were done using a strict clock model. The Markov chain Monte Carlo chain length was 50 000 000 for the divergence dating runs, and 100 000 000 for the EBSP runs, which resulted in effective sample sizes (ESS) >200 for the majority of the parameters in all runs. Runs of divergence dating and EBSP including all samples were done for both clock rates. Subsequently, separate runs of EBSP including only samples from the northern North Island, only samples from central New Zealand, and only samples from the South Island plus the Sub-Antarctic Islands were performed, also for both clock rates. Beast traces were visualized in Tracer v.1.7.1 (Rambaut *et al.*, 2018), tree files were summarized with TreeAnnotator (Bouckaert *et al.*, 2014), target trees were visualized with FigTree v.1.4.4 (Rambaut, 2018) and the EBSP was plotted with R, using the plotEBSP.R source code (available from Beast 2 tutorials).

To check if the topology of the *COI* phylogenetic tree was also recovered by other mitochondrial and nuclear markers, fragments of both the mitochondrial DNA (mtDNA) 16S rRNA gene and the nuclear ribosomal internal transcriber spacer (ITS-1) were sequenced in a subset of the individuals included in the *COI* analyses, representing all four geographical regions (northern North Island, central New Zealand, South Island and Sub-Antarctic Islands). The 16S PCR amplification used the primers 16Sar and 16Sbr (Palumbi, 1996), while for the ITS-1 PCRs, the primers used were 5.8c and 18d (Hillis & Dixon, 1991) (see Supporting Information for details). The ITS-1 tree included both alleles from each *O. neglectus* specimen. Heterozygotes were resolved using multiple forward and reverse sequences from each PCR fragment, and all were due to either single nucleotide polymorphisms or single indels. For both genes, a neighbour joining phylogenetic tree was built with HKY genetic distance, and 1000 bootstraps, and a Bayesian tree was constructed with MrBayes using as substitution model HKY85, rate variation invgamma, chain length 1 000 000, one heated chain, heated chain temperature 0.2, subsampling frequency of 1000, burn-in length of 1000, and the Unconstrained Branch Lengths option with default GammaDir. All trees used GenBank sequences from the most closely related species available as outgroups: *Tonicia forbesii* (KJ574081.1) for 16S, and *O. hirasei* (AB714504.1) for ITS-1.

### Combined assessments of genetic and shell shape patterns

As a way to jointly assess shell shape and genetic patterns, Blomberg's $K$ and Pagel's $\lambda$ phylogenetic signal tests were performed (Pagel, 1999; Blomberg *et al.*, 2003), using the R package Phytools (Revell, 2012). In this scenario, phylogenetic signal is the relationship between morphological similarity and phylogenetic relatedness. These tests examine if the phenotypic traits (the shape of each valve) are concordant with the phylogeny constructed with genetic data (Blomberg *et al.*, 2003; Münkemüller *et al.*, 2012).

The phylogeny used in the phylogenetic signal tests was a Bayesian *COI* phylogenetic tree constructed using the Geneious v.10.2.3 plug-in Mr. Bayes, with substitution model HKY85, rate variation invgamma, chain length 1 000 000, one heated chain, heated chain temperature 0.2, subsampling frequency of 1000 and burn-in length of 1000, and using the Unconstrained Branch Lengths option with default GammaDir. The traits tested for phylogenetic signal consisted of PC1 scores of valve shape, each valve being analysed separately (each valve as a different trait).

Tests of phylogenetic signal require that both types of data are available for all samples (in this case, genetic data from the *COI* gene, and the shell shape data obtained with geometric morphometrics), which resulted in each valve having a different sample size tested for phylogenetic signal.

To identify shape variables that maximize differences between genetic clades, a canonical discriminant analysis was performed, with the aim to visualize how far the genetic clades can be separated by the combined shape data of the three valves in each individual. First, a PCA was performed with the *COI* data using the R package LEA v.2.0 (Frichot & François, 2015). Then, the R package Candisc (Friendly & Fox, 2017) was used to perform a generalized canonical discriminant analysis, in which the genetic clades identified with the PCA on the *COI* data were used as a classifying factor, and the first principal components score of the shape of each valve were used as three response variables per individual. The resultant individual discriminant scores

from Candisc were plotted and identified according to genetic clades, using ggplot2 (Wickham, 2016).

To compare genetic and shape data and assess their association, a Procrustes superimposition was carried out using the R package vegan (Oksanen *et al.*, 2019). First, vegan was used to compute the Euclidean distances of the genetic and the shape PC1 scores, and then to determine the centroids for each population. With the population centroid data stored in a genetic and a morphological matrix, a Procrustes superimposition was carried out, and the residuals were plotted to visualize the association between the two matrices. The statistical significance of the Procrustean fit was assessed with 999 free permutations.

For each of the individuals included in the 16S tree, additional morphological and subspecies information was determined: shell pattern (ringed or smooth), morphogroup identified in the geometric morphometrics analyses, and also the subspecies-level classification of each individual (*O. neglectus neglectus* or *O. neglectus subantarcticus*) (O'Neill, 1985), based on the location from which they were sampled. The rationale for assigning shell patterns to individuals was based on visual observation of the most distinctive difference in shell pattern within the species: if concentric lines could be discerned in the valves, individuals were considered ringed, while individuals without discernible lines in the valves were considered smooth (Supporting Information, Fig. S1).

## RESULTS

### Shell shape variation

The elliptic Fourier analyses of shell shape for the fourth valve identified a northern morphogroup (northern North Island and central New Zealand) and a southern morphogroup (South Island and the Sub-Antarctic Islands). For the head and tail valves, however, morphogroups are not clearly distinguished in the PCA plots, as the confidence intervals overlap (Supporting Information, Fig. S2).

PCAs of the normalized elliptic Fourier descriptors show that PC1 is responsible for 69.73% (fourth), 62.75% (head) and 54.64% (tail) of the variation among samples, followed by 19.42% (fourth), 13.87% (head) and 15.00% (tail) in PC2, and 2.83% (fourth), 3.50% (head) and 7.61% (tail) in PC3.

The plot of the centroids of Euclidean distance for PC1 of all three valves distinguishes the same northern and southern morphogroups (Fig. 2). There is, however, great variation in shape within each population and morphogroup, as can be seen by the broad distribution of the points and large area of the polygons in the plot.

The results of Spearman's correlation tests of size and shape are consistent and show a significant positive correlation between size and shape for the fourth valve, and a significant and negative correlation for the head and the tail valve. However, the correlation coefficients are all relatively low ($\rho = 0.44$ for the fourth, $\rho = -0.18$

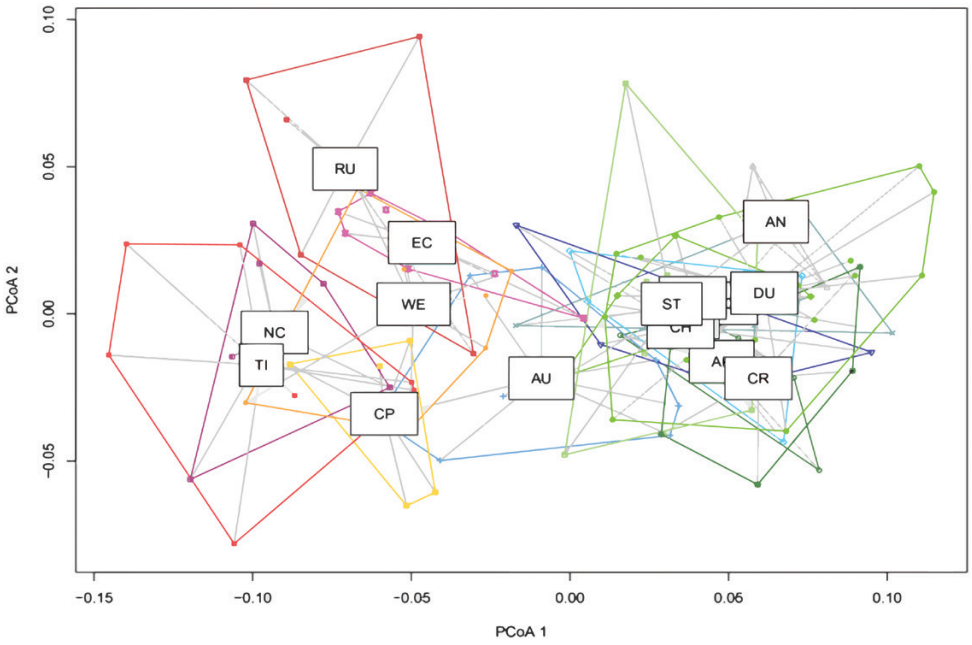


**Figure 2.** Plot of the morphometric Euclidean distance centroids for the first principal component analysis (PCoA) score of the head, tail and fourth valves combined. Individuals were grouped by sampling population. PCoA1 is responsible for 42.82% of the variation; PCoA2 is responsible for 10.49% of the variation.

for the head and $\rho = -0.32$ for the tail valve, $P < 0.05$ for all valves). The plot of PC1 and PC2 scores of the fourth valve for similar-sized individuals recovered the same pattern shown by all individuals in the complete dataset (Supporting Information, Figs S2-A, S3), with the northern and southern morphogroups. These results show that although there is some size–shape correlation and considerable intra-population variability in shape, the two morphogroups identified are delineating consistent morphological differences between geographical regions.

### Genetic structure, historical divergence and demography

The phylogenetic tree of the *COI* gene was built with 139 *O. neglectus* sequences and one outgroup *O. hirasei* sequence (Fig. 3A; Supporting Information, Fig. S4). There are three clearly supported clades (~9–10% divergence), corresponding to the northern North Island (Russell, Auckland, Coromandel and East Cape), central New Zealand (Wellington and Cape Palliser), and a southern group with all the South Island and Sub-Antarctic Islands populations, including the Chatham Islands (which are the most differentiated population in the southern group). The same overall topology was also recovered by both the 16S rRNA gene and the nuclear ITS-1 marker, with high support for the split into three clades, which are composed of the same above-mentioned populations (Fig. 4). In the *COI* tree, there is very strong support for combined monophyly of the central New Zealand and northern North Island clades, whereas the other two markers provide weak support for a sister relationship of southern and central clades. The inferred geographical range of the southern clade is considerably larger than that of either the northern North Island or the central New Zealand clades.

The haplotype network, as well as the population pairwise $\Phi_{ST}$, support the strong differentiation among populations of different genetic clades (Supporting Information, Fig. S5 and Table S2). In addition, the pairwise $\Phi_{ST}$ analyses clearly show stronger differentiation between populations within the northern North Island and central New Zealand clades (overall $\Phi_{ST} = 0.97$) than populations within the (much geographically broader) southern clade (overall $\Phi_{ST} = 0.38$).

The results of the divergence dating analyses suggest relatively old evolutionary splits for the three genetic clades. Specifically, considering the estimates derived from the upper and the lower divergence rates respectively, the clades are estimated to have diverged around 3–10 Mya. Considering the overlap in credible intervals of the node bars representing divergence time (Fig. 3A), the three clades could have diverged at around the same time within this interval. The skyline plot suggests a much more recent strong bottleneck, well after the clades diverged (Fig. 3B). This bottleneck is also seen within each group, when the analyses were carried out separately within groups (Supporting Information, Fig. S6).

### Combined genetic and shell shape patterns

Both Blomberg's $K$ and Pagel's $\lambda$ measures of phylogenetic signal (the relationship between morphological similarity and phylogenetic relatedness) are significant for all three valves (Table 2). The values of $K$ are relatively low, suggesting that although significant, the phylogenetic signal in the morphometric data is not strong. Pagel's $\lambda$ values indicate that shell shape most closely matches the *COI* relationships for the tail valve.

The northern and southern morphogroups are identified in the canonical discriminant analysis among genetic clades with some overlap (Fig. 5). The fourth and tail valve account for most of the separation between the two morphogroups, while the head valve is less important in this regard. The first canonical variate is responsible for 98.7% of the between-group differences, and the second canonical variate for only 1.3%.

The plot of the residuals from the Procrustes superimposition shows that the three genetic clades have well-separated vector origins, and the vector end-points depict the variation in the morphological data (Supporting Information, Fig. S7). Results from the permutation procedure show a significant and strong correlation between the superimposed genetic and shape matrices, as the correlation in a symmetric Procrustes rotation is 0.73 (analogous to an $R^2$ coefficient of determination), with $P < 0.05$.

The combined morphological, genetic and taxonomic information shows that the genetic clades and morphogroups (based on shell shape) do not match the shell pattern (ringed or smooth valves) and subspecies classification (Fig. 4). The southern shell shape morphogroup is entirely consistent with the southern genetic clade, but it includes both ringed and smooth patterns and both subspecies *O. neglectus neglectus* and *O. neglectus subantarticus*; the northern shell shape morphogroup includes individuals from two genetic clades (northern North Island and central New Zealand), but has only ringed patterned individuals that belong to the subspecies *O. neglectus neglectus*.

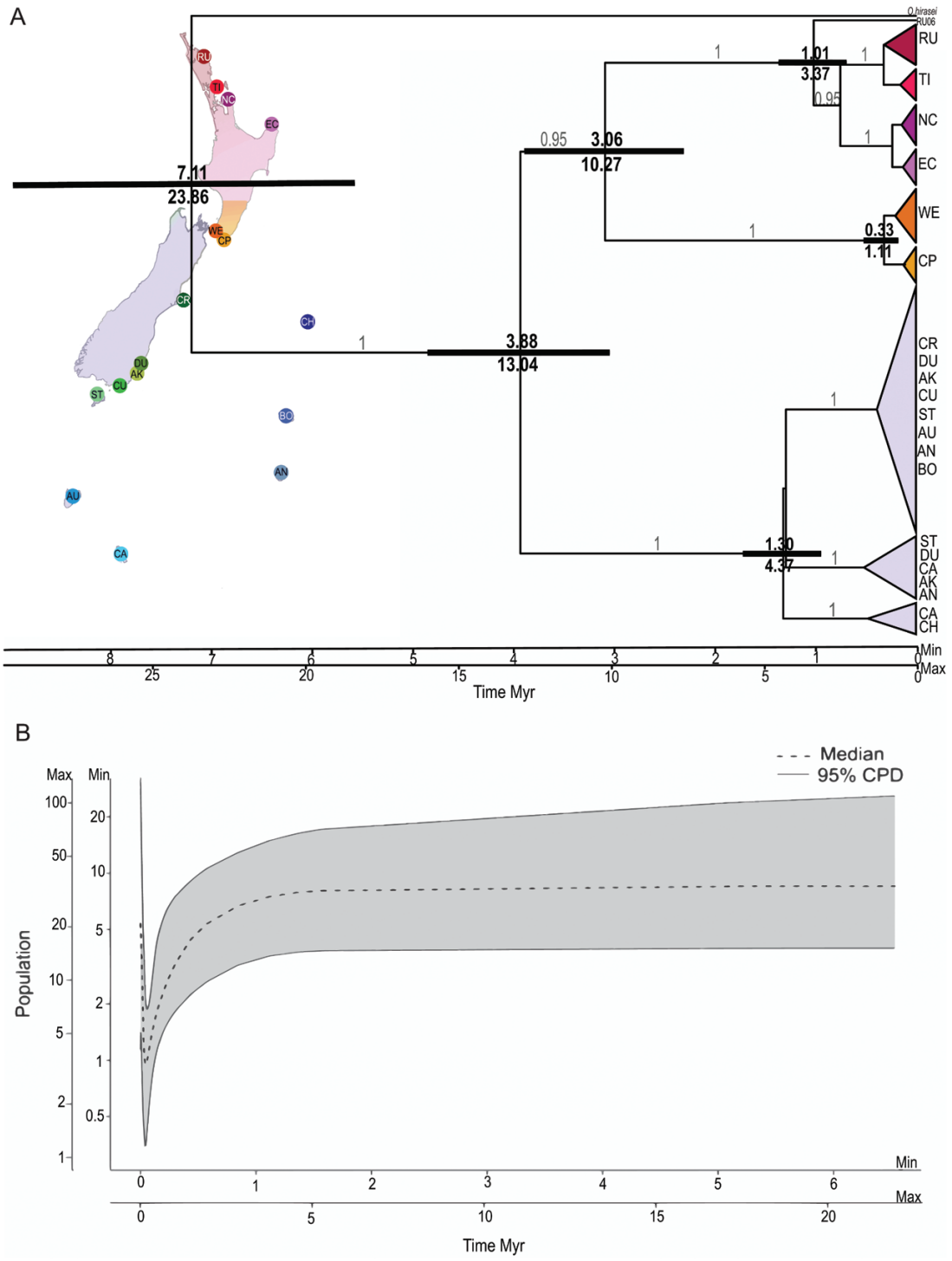


**Figure 3.** A, maximum clade credibility tree for *Onithochiton neglectus* mitochondrial *COI* haplotypes, showing estimated ages of clade MRCAs (most recent common ancestors). Each node bar includes the lower and upper mean divergence time estimates. The bar extension represents the 95% credible interval. Timelines are in million years before the present, where 0 is present time. The top timeline is relative to the highest divergence rate, and the bottom timeline is relative to the lowest divergence rate. Labels on the branches show the posterior support for the clades. B, *O. neglectus* extended Bayesian skyline plot. Time (*x* axis) is in million years, with zero corresponding to present time. The *y* axis shows population size estimates (right *y* axis for highest evolutionary rate and left *y* axis for lowest evolutionary rate).

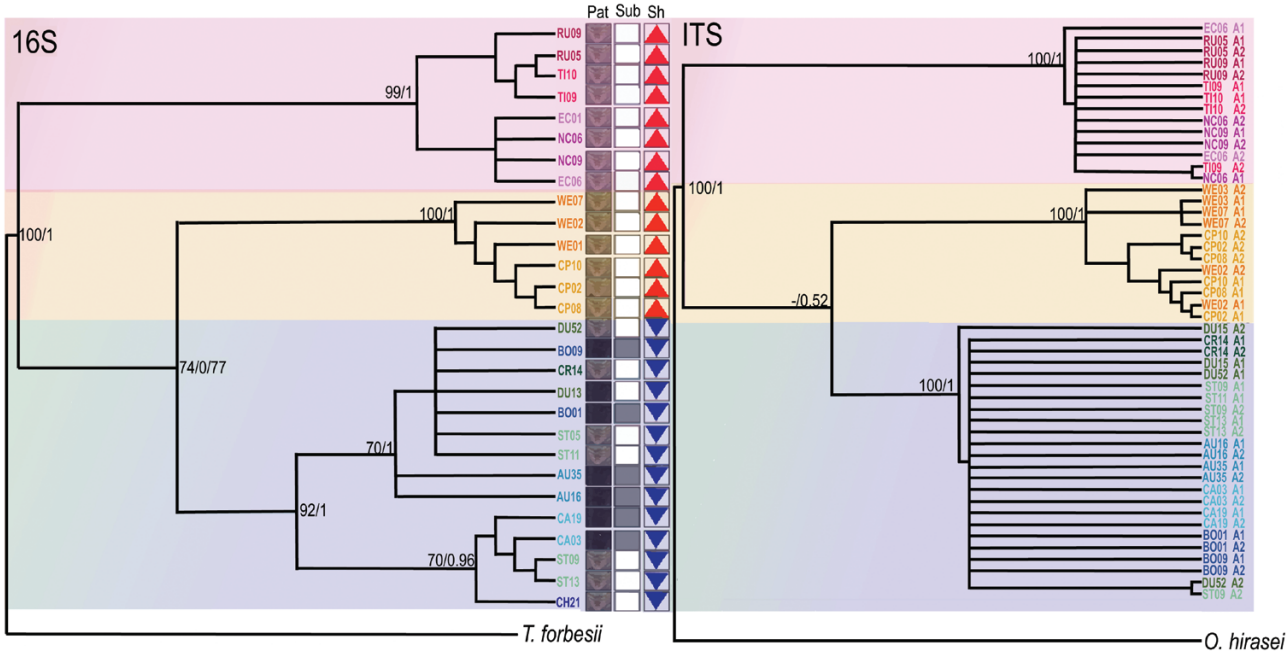


**Figure 4.** Phylogenetic relationships among individuals inferred from 16S rRNA and ITS-1 sequences, along with their morphological and taxonomic classifications. Individual identifiers are coloured by sampling population, and use the sample codes as in Figure 1 and Table 1. Background colours identify genetic clades. Node labels show percentage neighbour-joining branch support followed by Bayesian posterior probability. Non-genetic data are included for each individual in the 16S tree: 'Pat' (pattern) indicates the presence/absence of rings on the shell; 'Sub' (subspecies) indicates to which subspecies individuals would be classified (empty square, *O. neglectus neglectus*; filled square, *O. neglectus subantarcticus*); 'Sh' (shape) indicates to which morphogroup individuals were classified in the geometric morphometrics analysis (upward triangle, northern morphogroup; downward triangle, southern morphogroup).

## DISCUSSION

### Spatial distribution of shape and genetic variation

Throughout its southern distribution, *O. neglectus* is predominantly found in *Durvillaea* holdfasts, whereas in the North Island it is predominantly found under rocks, not associated with kelp (Morton & Miller, 1973; Creese, 1988). In this study, using a more thorough sampling of the biogeographical range of *O. neglectus* than previously (Nikula *et al.*, 2012; Waters *et al.*, 2018a), we detected distinct northern and southern *O. neglectus* morphogroups based on shell shape. Our molecular analyses confirmed the existence of a single broad southern genetic lineage, which matches the distribution of the southern morphogroup, and exhibits little geographical sub-structure. In contrast, the northern morphogroup has strong genetic subdivisions, comprising two major geographically distinct genetic lineages, each of which presents strong fine-scale phylogeographical structure among all sampled populations. The geographical distribution of the broad southern morphogroup and southern genetic lineage is completely concordant with the region where kelp association dominates, but does not match the previous subspecies distinction. These patterns of shape and genetic variation match our initial predictions, and strongly implicate kelp-rafting by chitons as a major force impacting the evolution of this species. It appears that, in the absence of a major mechanism of dispersal, the brooding life history of this species leads to extreme phylogeographical structuring among locations, and this is observed throughout the northern distribution of the species. Throughout the broad southern distribution, where rafting on kelp appears to provide a potent means of dispersal, on-going gene flow appears to have effectively homogenized genetic variation, and a distinct morphogroup has differentiated.

*Onithochiton neglectus* hatches from the brood as ciliated larvae, but individuals settle immediately if a suitable substrate is available (Creese, 1986). As a brooding species with limited mobility, low gene flow among populations is expected (O'Neill, 1985; Creese, 1986; Nikula *et al.*, 2012). The detection of strong phylogeographical structuring is commonly thought to be a consequence of this reproductive behaviour, unless rafting dispersal breaks this pattern (Thiel & Haye,

**Table 2.** Phylogenetic signal for the shape of the three valves, using the COI phylogenetic tree

| Valve | Blomberg's *K* | *P* | Pagel's λ | LogL | LogL0 | *P* |
|---|---|---|---|---|---|---|
| Fourth | 0.214 | 0.001 | 0.590 | 168.20 | 136.19 | 1.23 e-15 |
| Head | 0.093 | 0.004 | 0.437 | 247.34 | 223.64 | 5.76 e-12 |
| Tail | 0.119 | 0.001 | 0.825 | 268.07 | 250.36 | 9.48 e-10 |

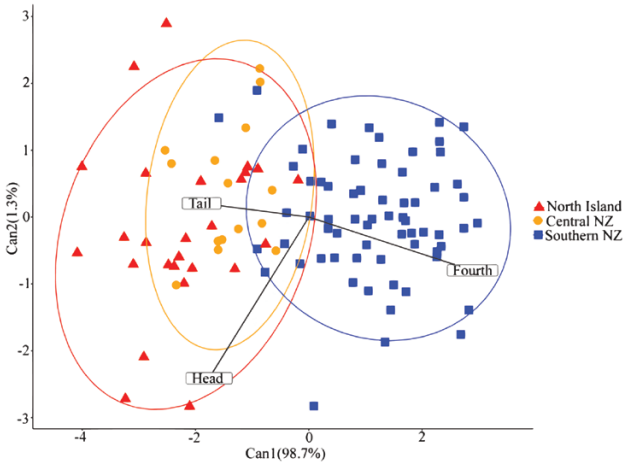


**Figure 5.** Discriminant analysis plot showing the combined morphological differences among the three genetic clades. Individual canonical scores are points coloured by genetic clade identity; canonical structure coefficients are vectors displaying the fourth, head and tail coefficients, starting at the origin. The *x* axis shows the first canonical variate (Can1); the *y* axis shows the second canonical variate (Can2).

2006). Kelp-rafting has been shown to be a driver of gene flow in several brooding species, including *O. neglectus* (Helmuth *et al.*, 1994; Fraser *et al.*, 2011; Nikula *et al.*, 2012; Waters *et al.*, 2018b), and can connect species across the Southern Ocean when carried by the Antarctic Circumpolar Current (Cumming *et al.*, 2014). Although this mode of connectivity is clearly important along New Zealand's South Island and throughout the Sub-Antarctic Islands, floating kelp is unlikely to be such a dominant force in the northern North Island and central New Zealand regions. The predominant direction of coastal marine currents probably hinders northward movement of southern *Durvillaea* rafts towards the North Island of New Zealand, where *D. poha* is absent, and *D. antarctica* is much less frequent, and forms a distinct northern genetic lineage (Fraser *et al.*, 2009; Collins *et al.*, 2010; Bussolini & Waters, 2015). Furthermore, although possible, an association of *O. neglectus* with holdfasts of other algae species has never been reported, nor observed by us. As a result, kelp-rafting is far less likely to promote successful gene flow among northern North Island and central New Zealand *O. neglectus* populations than among South Island and Sub-Antarctic Islands. This appears to be confirmed by all our genetic results, showing much greater differentiation throughout the North Island than throughout the far more extensive southern region.

The degree of concordance between shell shape and the genetic results is recovered in the phylogenetic signal tests, in which *K* and λ are small but significant. These tests indicate that the shape of each valve matches the *COI* phylogeny to a large extent, but also reflect the existence of the central genetic clade, undetected by the shell shape analyses, as well as considerable within-population shell shape variation. The discriminant analysis and the Procrustes superimposition also reflect the strong association between the genetic and shape data. In addition, although these analyses highlight that valve shape is highly variable, the shape of the fourth and tail valves could be promising diagnostic characters to discern the southern genetic clade from the other two clades.

The combined analyses of genetic and shape data reveal a unique shell shape within the southern clade, and a shared shell shape between the northern North Island and central New Zealand clades. Although the differences in shell shape may be due to entirely neutral processes, the striking concordance leads us to speculate that shell shape in *O. neglectus* could be an adaptive trait, corresponding to the characteristics of the environment they inhabit (e.g. dominated by or lacking *D. antarctica* and *D. poha*). Shell shape has been considered an adaptive trait in several mollusc species, such as in two ecotypes of the marine snail *Littorina saxatilis* (Kess & Boulding, 2019). However, defining the exact factors acting as selective agents is challenging (Verhaegen *et al.*, 2019), and testing for local adaptation is outside the scope of this study.

### Palaeo-ecology and clade divergence

Our estimates of divergence times were based on the best available *COI* substitution rate calculations from related chitons, using minimum and maximum estimates of species divergence times across the Panama Isthmus (García-Ríos *et al.*, 2014). These result in estimates of *O. neglectus* clade divergence

times of around 3–10 Mya, although these are likely to be over-estimates due to the time-dependent rate effect (Ho *et al.*, 2011).These divergence times are consistent with either between-population or between-species chiton divergences, depending on the taxonomic group (García-Ríos *et al.*, 2014). The divergence times are also similar to what has been estimated for other brooding species in the Southern Ocean, such as sea stars and limpets (González-Wevar *et al.*, 2018; Moreau *et al.*, 2019), and may be associated with climate fluctuations during the Plio-Pleistocene (Naish, 2005).

The skyline plot (EBSP) suggests that *O. neglectus* had a very recent and profound bottleneck and population expansion, and this was evident within all clades, but was much more recent than the origin of the three clades. Such recent bottlenecks may be coincident with the Last Glacial Maximum, around 27 kya for the Southern Ocean (Suggate & Almond, 2005). The distribution of *D. antarctica* was greatly impacted during the Last Glacial Maximum, when the most southerly populations were probably eliminated by ice-scour (Fraser *et al.*, 2009, 2010). However, the specific impact of past *D. antarctica* range shifts on *O. neglectus* populations are unclear. The distribution of *D. antarctica* in regions north of the Campbell Islands is unlikely to have been reduced by ice scouring (Fraser *et al.*, 2009), but southern rafting kelp may have been driven further north by the northern movement of the sub-tropical front (Sikes *et al.*, 2009; Bostock *et al.*, 2015). Thus, changes in the patterns of kelp-rafting may have impacted past population connectivity throughout the historical range of *O. neglectus*, but it is speculative to predict what these changes may have been without additional detail.

### The use of elliptic Fourier analyses in chitons

Geometric morphometric methodologies are widely applied in shell shape assessments of varied molluscs, such as bivalves and gastropods (Vaux *et al.*, 2017; Gemmell *et al.*, 2018; Perez & Santelli, 2018), but have been rarely used in chitons. The use of elliptic Fourier descriptors to undertake geometric morphometrics analyses in chiton valves seems appropriate, as the valve outline describes a closed contour, and there are few structures on the exterior of each valve that could reliably be used as type 1 landmarks for a Procrustes superimposition (Zelditch *et al.*, 2012). The intersection between the apophysis and the valves could be used to determine landmarks, although the head valve does not have apophysis. Alternatively, the ventral side of the valves should provide more homologous structures to be used as landmarks, but this is only an option when disarticulating the valves and causing permanent damage to specimens is not of concern. Elliptic Fourier descriptors have been applied to shape analyses on other structures with presumably few type 1 landmarks, such as fish otoliths, jellyfish statoliths, rice grains and radish roots (Iwata *et al.*, 1998; Paul *et al.*, 2013; Iwata *et al.*, 2015; Mooney & Kingsford, 2016). In addition, shape analyses considering single valves, instead of the whole animal, are a valuable alternative when working with ethanol-preserved chitons, as these specimens are usually curved, and flattening them is likely to damage the valves.

### Taxonomic implications

Given previous taxonomic classifications based on morphology and geographical range (O'Neill, 1985), we expected that the shell shape analyses would distinguish *O. neglectus subantarcticus* from *O. neglectus neglectus*. However, there is no concordance in the classification of individuals under genetic, shell shape, shell pattern and subspecies categories (Fig. 4).

In the southern region, geography is important in defining *O. neglectus subantarcticus*, which was described from the Antipodes Islands, Auckland Islands, Campbell Islands and possibly Bounty Islands, as having a smooth and dark shell with less morphological variation than *O. neglectus neglectus* found elsewhere (O'Neill, 1985). Our results show that the broad southern morphogroup is composed of samples from the described *O. neglectus subantarcticus* range as well as from throughout the South Island, Auckland Islands, Campbell Islands and Chatham Islands. Thus, shell shape and molecular patterns refute the existence of a subspecies of *O. neglectus* confined to the above-mentioned Sub-Antarctic Islands, and do not support the current taxonomic subdivision of *O. neglectus* into these two subspecies.

It is possible that either the two morphogroups or the three genetic clades described here could be considered subspecies or even species. In central New Zealand, the Cook Strait region (between the North and South Islands) has complex circulation (Bowman *et al.*, 1983), and it may act as a barrier to *O. neglectus* connectivity, as it appears to do for other marine invertebrates (Ross *et al.*, 2009; Veale & Lavery, 2011; Will *et al.*, 2011, 2015; Ross *et al.*, 2012; Nagel *et al.*, 2015). However, although the current sampling is sufficient to expose some of the major evolutionary patterns within *O. neglectus*, it is not sufficient to address taxonomic revision. This study lacks samples to the north and south of the central genetic clade, and thus cannot determine if intermediate genetic lineages exist in these regions. There are also other portions of the species' distribution that have not been sampled (such as the west coast), where additional cryptic genetic lineages may be found. Thus, a taxonomic revision is currently premature, and further study is

required to determine if the three clades defined here are representative of the entire species.

## CONCLUSION

Overall, the shape and genetic results presented here reveal a contrasting pattern between northern and southern *O. neglectus*. Such a contrast emphasizes the role of kelp-rafting in connecting populations that would otherwise evolve in isolation, and allows a glimpse into what may be the future evolutionary trajectories of these populations if kelp distribution and extent of rafting change as a response to ocean warming. Further investigation of genomic markers and their correlation with environmental factors will shed light on the potential impact of selection and adaptation in driving the observed pattern of variation within this species.

## ACKNOWLEDGEMENTS

We thank Prof. Hamish Spencer, Dr Ceridwen Fraser and Dr Raisa Nikula for obtaining samples from the South Island and Sub-Antarctic Islands, and Dr Tania King for sorting and shipping these samples. We also thank Airton C. Agostinho, Dr. Bryce Peebles, Sarah Brand, and Dr Dyahruri Sanjayasarit for assistance in collecting samples, and Dr Vibha Thakur for help in the wet laboratory. We also thank Prof. Martin Thiel and an anonymous reviewer for helpful comments on the manuscript. We thank Prof. Mary Morgan-Richards for her advice on geometric morphometric methods. We also thank the New Zealand Department of Conservation. This research was supported by the School of Biological Sciences of the University of Auckland, and a Systematic Research Fund award from both the Linnean Society of London and the Systematics Association.

## REFERENCES

**Adams DC**, **Rohlf FJ**, **Slice DE. 2004.** Geometric morphometrics: ten years of progress following the 'revolution'. *Italian Journal of Zoology* **71:** 5–16.

**Baxter JM**, **Jones AM. 1981.** Valve structure and growth in the chiton *Lepidochitona cinereus* (Polyplacophora: Ischnochitonidae). *Journal of the Marine Biological Association of the United Kingdom* **61:** 65.

**Blomberg SP**, **Garland TJ**, **Ives AR. 2003.** Testing for phylogenetic signal in comparative data: behavioral traits are more liable. *Evolution* **54:** 717–745.

**Bostock HC**, **Hayward BW**, **Neil HL**, **Sabaa AT**, **Scott GH. 2015.** Changes in the position of the Subtropical Front south of New Zealand since the last glacial period. *Paleoceanography* **30:** 824–844.

**Bouckaert RR**, **Drummond AJ. 2017.** bModelTest: Bayesian phylogenetic site model averaging and model comparison. *BMC Evolutionary Biology* **17:** 42.

**Bouckaert R**, **Heled J**, **Kühnert D**, **Vaughan T**, **Wu C-H**, **Xie D**, **Suchard MA**, **Rambaut A**, **Drummond AJ. 2014.** BEAST 2: a software platform for Bayesian evolutionary analysis. *PLoS Computational Biology* **10:** e1003537.

**Bowman MJ**, **Kibblewhite AC**, **Murtagh RA**, **Chiswell SM**, **Sanderson BG. 1983.** Circulation and mixing in greater Cook Strait, New Zealand. *Oceanologica Acta* **6:** 383–391.

**Bussolini LT**, **Waters JM. 2015.** Genetic analyses of rafted macroalgae reveal regional oceanographic connectivity patterns. *Journal of Biogeography* **42:** 1319–1326.

**Cadrin SX. 2010.** Stock identification of marine populations. In: Elewa AMT, ed. *Morphometrics for Nonmorphometricians*. Berlin: Springer**,** 219–232.

**Christie H**, **Gundersen H**, **Rinde E**, **Filbee-Dexter K**, **Norderhaug KM**, **Pedersen T**, **Bekkby T**, **Gitmark JK**, **Fagerli CW. 2019.** Can multitrophic interactions and ocean warming influence large-scale kelp recovery? *Ecology and Evolution* **9:** 2847–2862.

**Collins CJ**, **Fraser CI**, **Ashcroft A**, **Waters JM. 2010.** Asymmetric dispersal of southern bull-kelp (*Durvillaea antarctica*) adults in coastal New Zealand: testing an oceanographic hypothesis. *Molecular Ecology* **19:** 4572–4580.

**Cooke SB**, **Terhune CE. 2015.** Form, function, and geometric morphometrics. *The Anatomical Record* **298:** 5–28.

**Creese RG. 1986**. Brooding behaviour and larval development in the New Zealand chiton, *Onithochiton neglectus* de Rochebrune (Mollusca: Polyplacophora). *New Zealand Journal of Zoology* **13:** 83–91.

**Creese RG. 1988.** Ecology of molluscan grazers and their interactions with marine algae in north-eastern New Zealand: a review. *New Zealand Journal of Marine and Freshwater Research* **22:** 427–444.

**Cumming RA**, **Nikula R**, **Spencer HG**, **Waters JM**, **Crame A. 2014.** Transoceanic genetic similarities of kelp-associated sea slug populations: long-distance dispersal via rafting? *Journal of Biogeography* **41:** 2357–2370.

**Excoffier L**, **Lischer HEL. 2010.** Arlequin suite ver 3.5: a new series of programs to perform population genetics analyses under Linux and Windows. *Molecular Ecology Resources* **10:** 564–567.

**Folmer O**, **Black MA**, **Hoeh W**, **Lutz R**, **Vrijenhoek R. 1994.** DNA primers for amplification of mitochondrial cytochrome c oxidase subunit I from diverse metazoan invertebrates. *Molecular Marine Biology and Biotechnology* **3:** 294–299.

**Fraser CI**, **Nikula R**, **Spencer HG**, **Waters JM. 2009.** Kelp genes reveal effects of subantarctic sea ice during the Last Glacial Maximum. *Proceedings of the National Academy of Sciences USA* **106:** 3249–3253.

**Fraser CI**, **Nikula R**, **Waters JM. 2011.** Oceanic rafting by a coastal community. *Proceedings of the Royal Society B* **278:** 649–655.

**Fraser CI**, **Thiel M**, **Spencer HG**, **Waters JM. 2010.** Contemporary habitat discontinuity and historic glacial ice

drive genetic divergence in Chilean kelp. *BMC Evolutionary Biology* **10:** 1–12.

**Frichot E**, **François O. 2015.** LEA: an R package for landscape and ecological association studies. *Methods in Ecology and Evolution* **6:** 925–929.

**Friendly M**, **Fox J. 2017.** *candisc: visualizing generalized canonical discriminant and canonical correlation analysis*. Available at: https://CRAN.R-project.org/package=candisc

**García-Ríos CI**, **Pérez-Pérez NM**, **Fernández-López J**, **Fuentes FA. 2014.** Calibrating the chitons (Mollusca: Polyplacophora) molecular clock with the mitochondrial DNA cytochrome C oxidase I gene. *Revista de Biología Marina y Oceanografía* **49:** 193–207.

**Gemmell MR**, **Trewick SA**, **Crampton JS**, **Vaux F**, **Hills SFK**, **Daly MJ**, **Marshall BA**, **Beu AG**, **Morgan-Richards M. 2018.** Genetic structure and shell shape variation within a rocky shore whelk suggest both diverging and constraining selection with gene flow. *Biological Journal of the Linnean Society* **125:** 827–843.

**González-Wevar CA**, **Segovia NI**, **Rosenfeld S**, **Ojeda J**, **Hüne M**, **Naretto J**, **Saucède T**, **Brickle P**, **Morley S**, **Féral J**, **Spencer HG**, **Poulin E. 2018.** Unexpected absence of island endemics: long-distance dispersal in higher latitude sub-Antarctic Siphonaria (Gastropoda: Euthyneura) species. *Journal of Biogeography* **45:** 874–884.

**Helmuth B**, **Veit RR**, **Holberton R. 1994.** Long-distance dispersal of a subantarctic brooding bivalve (*Gaimardia trapesina*) by kelp-rafting. *Marine Biology* **120:** 421–426.

**Hillis DM**, **Dixon MT. 1991.** Ribosomal DNA: molecular evolution and phylogenetic inference. *The Quarterly Review of Biology* **66:** 411–453.

**Ho SY**, **Lanfear R**, **Bromham L**, **Phillips MJ**, **Soubrier J**, **Rodrigo AG**, **Cooper A. 2011.** Time-dependent rates of molecular evolution. *Molecular Ecology* **20:** 3087–3101.

**Iwata H**, **Ebana K**, **Uga Y**, **Hayashi T. 2015.** Genomic prediction of biological shape: elliptic Fourier analysis and kernel partial least squares (PLS) regression applied to grain shape prediction in rice (*Oryza sativa* L.). *PLoS One* **10:** e0120610.

**Iwata H**, **Niikura S**, **Matsuura S**, **Takano Y**, **Ukai Y. 1998.** Evaluation of variation of root shape of Japanese radish (*Raphanus sativus* L.) based on image analysis using elliptic Fourier descriptors. *Euphytica* **102:** 143–149.

**Iwata H**, **Ukai Y. 2002.** SHAPE: a computer program package for quantitative evalutaion of biological shapes based on elliptic Fourier descriptors. *The Journal of Heredity* **93:** 384–385.

**Kassambara A. 2018.** *ggpubr: 'ggplot2' based publication ready plots*. Available at: https://CRAN.R-project.org/package=ggpubr

**Kess T**, **Boulding EG. 2019.** Genome-wide association analyses reveal polygenic genomic architecture underlying divergent shell morphology in Spanish *Littorina saxatilis* ecotypes. *Ecology and Evolution* **9:** 1–15.

**Kuhl FP**, **Giardina CR. 1982.** Elliptic fourier features of a closed contour. *Computer Graphics and Image Processing* **18:** 236–258.

**Leigh JW**, **Bryant D. 2015.** PopART: Full-feature software for haplotype network construction. *Methods in Ecology and Evolution* **6:** 1110–1116.

**López BA**, **Macaya EC**, **Rivadeneira MM**, **Tala F**, **Tellier F**, **Thiel M. 2018.** Epibiont communities on stranded kelp rafts of *Durvillaea antarctica* (Fucales, Phaeophyceae) – Do positive interactions facilitate range extensions? *Journal of Biogeography* **45:** 1833–1845.

**López BA**, **Tellier F**, **Retamal-Alarcón JC**, **Pérez-Araneda K**, **Fierro AO**, **Macaya EC**, **Tala F**, **Thiel M. 2017.** Phylogeography of two intertidal seaweeds, *Gelidium lingulatum* and *G. rex* (Rhodophyta: Gelidiales), along the South East Pacific: patterns explained by rafting dispersal? *Marine Biology* **164:** 188.

**Mooney CJ**, **Kingsford MJ. 2016.** Statolith morphometrics as a tool to distinguish among populations of three cubozoan species. *Hydrobiologia* **787:** 111–121.

**Moreau C**, **Danis B**, **Jossart Q**, **Eleaume M**, **Sands C**, **Achaz G**, **Aguera A**, **Saucede T. 2019.** Is reproductive strategy a key factor in understanding the evolutionary history of Southern Ocean Asteroidea (Echinodermata)? *Ecology and Evolution* **9:** 8465–8478.

**Morton J**, **Miller M. 1973.** *The New Zealand sea shore*. Glasgow: Collins.

**Münkemüller T**, **Lavergne S**, **Bzeznik B**, **Dray S**, **Jombart T**, **Schiffers K**, **Thuiller W. 2012.** How to measure and test phylogenetic signal. *Methods in Ecology and Evolution* **3:** 743–756.

**Nagel MM**, **Sewell MA**, **Lavery SD. 2015.** Differences in population connectivity of a benthic marine invertebrate *Evechinus chloroticus* (Echinodermata: Echinoidea) across large and small spatial scales. *Conservation Genetics* **16:** 965–978.

**Naish TR. 2005.** New Zealand`s shallow-marine record of Pliocene-Pleistocene global sea-level and climate change. *Journal of the Royal Society of New Zealand* **35:** 1–8.

**Nikula R**, **Spencer HG**, **Waters JM. 2011.** Evolutionary consequences of microhabitat: population-genetic structuring in kelp- vs. rock-associated chitons. *Molecular Ecology* **20:** 4915–4924.

**Nikula R**, **Spencer HG**, **Waters JM. 2012.** Passive rafting is a powerful driver of transoceanic gene flow. *Biology Letters* **9:** 20120821.

**O'Neill MHB. 1984.** Morphological changes in *Onithochiton neglectus* Rochebrune, 1881 (Mollusca: Chitonidae), and their taxonomic significance. *New Zealand Journal of Zoology* **11:** 43–48.

**O'Neill MHB. 1985.** A review of the living New Zealand members of *Onithochiton* Gray, 1847 (Mollusca: Polyplacophora). *New Zealand Journal of Zoology* **12:** 141–154.

**Oksanen J**, **Blanchet FG**, **Friendly M**, **Kindt R**, **Legendre P**, **McGlinn D**, **Minchin PR**, **O'Hara RB**, **Simpson GL**, **Solymos P**, **Stevens MHH**, **Szoecs E**, **Wagner H. 2019.** *vegan: community ecology package*. Available at: https://CRAN.R-project.org/package=vegan

**Outomuro D**, **Johansson F. 2017.** A potential pitfall in studies of biological shape: does size matter? *Journal of Animal Ecology* **86:** 1447–1457.

**Pagel M. 1999.** Inferring the historical patterns of biological evolution. *Nature* **401:** 877–884.

**Palumbi SR. 1996.** Nucleic acids II: The polymerase chain reaction. In: Hillis DM, Moritz C, Mable BK, eds. *Molecular systematics*. Sunderland: Sinauer Associates, 205–247.

**Paul K**, **Oeberst R**, **Hammer C. 2013.** Evaluation of otolith shape analysis as a tool for discriminating adults of Baltic cod stocks. *Journal of Applied Ichthyology* **29:** 743–750.

**Perez DE**, **Santelli MB. 2018.** Allometric shell growth in infaunal burrowing bivalves: examples of the archiheterodonts *Claibornicardia paleopatagonica* (Ihering, 1903) and *Crassatella kokeni* Ihering, 1899. *PeerJ* **6:** e5051.

**Powell AWB. 1979.** *New Zealand Mollusca: marine, land, and freshwater shells.* London: Collins.

**Rambaut A. 2018.** *FigTree: tree figure drawing tool*, *1.4.4 edn*. Edinburgh: University of Edinburgh.

**Rambaut A**, **Drummond AJ**, **Xie D**, **Baele G**, **Suchard MA. 2018.** Posterior summarization in Bayesian phylogenetics using Tracer 1.7. *Systematic Biology* **67:** 901–904.

**Revell LJ. 2012.** phytools: an R package for phylogenetic comparative biology (and other things). *Methods in Ecology and Evolution* **3:** 217–223.

**Ross PM**, **Hogg ID**, **Pilditch CA**, **Lundquist CJ. 2009.** Phylogeography of New Zealand's coastal benthos. *New Zealand Journal of Marine and Freshwater Research* **43:** 1009–1027.

**Ross PM**, **Hogg ID**, **Pilditch CA**, **Lundquist CJ**, **Wilkins RJ. 2012.** Population genetic structure of the New Zealand estuarine clam *Austrovenus stutchburyi* (Bivalvia: Veneridae) reveals population subdivision and partial congruence with biogeographic boundaries. *Estuaries and Coasts* **35:** 143–154.

**Sheets HD**, **Covino KM**, **Panasiewicz JM**, **Morris SR. 2006.** Comparison of geometric morphometric outline methods in the discrimination of age-related differences in feather shape. *Frontiers in Zoology* **3:** 15.

**Sikes EL**, **Howard WR**, **Samson CR**, **Mahan TS**, **Robertson LG**, **Volkman JK. 2009.** Southern Ocean seasonal temperature and Subtropical Front movement on the South Tasman Rise in the late Quaternary. *Paleoceanography* **24:** 1–13.

**Smale DA**, **Wernberg T**, **Oliver ECJ**, **Thomsen M**, **Harvey BP**, **Straub SC**, **Burrows MT**, **Alexander LV**, **Benthuysen JA**, **Donat MG**, **Feng M**, **Hobday AJ**, **Holbrook NJ**, **Perkins-Kirkpatrick SE**, **Scannell HA**, **Sen Gupta A**, **Payne BL**, **Moore PJ. 2019.** Marine heatwaves threaten global biodiversity and the provision of ecosystem services. *Nature Climate Change* **9:** 306–312.

**Suggate RP**, **Almond PC. 2005.** The Last Glacial Maximum (LGM) in western South Island, New Zealand: implications for the global LGM and MIS 2. *Quaternary Science Reviews* **24:** 1923–1940.

**Thiel M**, **Haye PA. 2006.** The ecology of rafting in the marine environment. III. Biogeographical and evolutionary consequences. *Oceanography and Marine Biology Annual Review* **44:** 323–429.

**Vaux F**, **Crampton JS**, **Marshall BA**, **Trewick SA**, **Morgan-Richards M. 2017.** Geometric morphometric analysis reveals that the shells of male and female siphon whelks *Penion chathamensis* are the same size and shape. *Molluscan Research* **37:** 194–201.

**Veale AJ**, **Lavery SD. 2011.** Phylogeography of the snakeskin chiton *Sypharochiton pelliserpentis* (Mollusca: Polyplacophora) around New Zealand: are seasonal near-shore upwelling events a dynamic barrier to gene flow? *Biological Journal of the Linnean Society* **104:** 552–563.

**Verhaegen G**, **Herzog H**, **Korsch K**, **Kerth G**, **Brede M**, **Haase M. 2019.** Testing the adaptive value of gastropod shell morphology to flow: a multidisciplinary approach based on morphometrics, computational fluid dynamics and a flow tank experiment. *Zoological Letters* **5:** 1–13.

**Waters JM**, **King TM**, **Fraser CI**, **Craw D. 2018a.** An integrated ecological, genetic and geological assessment of long-distance dispersal by invertebrates on kelp rafts. *Frontiers of Biogeography* **10:** 1–13.

**Waters JM**, **King TM**, **Fraser CI**, **Garden CJ. 2018b.** Rafting dispersal in a brooding southern sea star (Asteroidea: Anasterias). *Invertebrate Systematics* **32:** 253.

**Wickham H. 2016.** *ggplot2: elegant graphics for data analysis*. New York: Springer.

**Will M**, **Hale ML**, **Schiel DR**, **Gemmell NJ. 2011.** Low to moderate levels of genetic differentiation detected across the distribution of the New Zealand abalone, *Haliotis iris*. *Marine Biology* **158:** 1417–1429.

**Will M**, **McCowan T**, **Gemmell NJ. 2015.** Broad-scale genetic patterns of New Zealand abalone, *Haliotis iris*, across a distribution spanning 13 degrees latitude and major oceanic water masses. *Genetica* **143:** 487–500.

**Zelditch ML**, **Swiderski DL**, **Sheets HD. 2012.** Landmarks and Semilandmarks. In Zelditch, ML, Swiderski, DL, Sheets HD, eds. Geometric Morphometrics for Biologists, 2nd edn. Academic Press, 23-50. ISBN 9780123869036. Available at http://www.sciencedirect.com/science/article/pii/B9780123869036000022

## SUPPORTING INFORMATION

Additional Supporting Information may be found in the online version of this article at the publisher's web-site:

Additional methodological details

**Table S1.** Additional information regarding collection sites, dates and sample sizes.

**Table S2.** Population pairwise $\Phi_{ST}$.

**Table S3.** Kruskal–Wallis results checking the size range of animals among regions.

**Figure S1.** Images of the three valves used in the geometric morphometrics analyses.

**Figure S2.** Plot of the first and second principal component scores (PC1 and PC2) of the shell shape analyses, coloured by regions.
**Figure S3.** Plot of the first and second principal component scores for the fourth valve of similar-sized individuals.
**Figure S4.** Phylogenetic relationships among individuals inferred from mitochondrial *COI* sequences.
**Figure S5.** *COI* haplotype network.
**Figure S6.** *Onithochiton neglectus* extended Bayesian skyline plot within the North Island clade (A and B), within the central New Zealand clade (C and D), and within the southern clade (E and F).
**Figure S7.** Plot of the residuals from the Procrustes superimposition, showing the three genetic clusters (origin of the vectors) and the spread in the morphological data (direction and length of the vectors).
**Figure S8.** Boxplot of valve area ($mm^2$) by region, to visualize differences in valve size among regions.

## SHARED DATA

Morphological data is available on figshare: doi:10.17608/k6.auckland.12291200.
Genetic data is available on GenBank: accession numbers MT434147 - MT434285 (COI); MT434702 - MT434751 (ITS-1); MT433888 - MT433915 (16S).